CrystEngComm

Effect of Halogen Substitution on Energies and Dynamics of Reversible Photomechanical Crystals Based on 9-Anthracenecarboxylic Acid

Journal:	*CrystEngComm*
Manuscript ID	CE-ART-06-2021-000846.R1
Article Type:	Paper
Date Submitted by the Author:	31-Jul-2021
Complete List of Authors:	Gately, Thomas; University of California Riverside, Chemistry Sontising, Watit; University of California Riverside, Dept. of Chemistry Easley, Connor; University of California, Riverside, Chemistry Islam, Imadule; King Saud bin Abdulaziz University for Health Sciences Al-Kaysi, Rabih; King Saud bin Abdulaziz University for Health Sciences, Basic Sciences Beran, Gregory; University of California Riverside, Chemistry Bardeen, Christopher; University of California at Riverside, Chemistry

Effect of Halogen Substitution on Energies and Dynamics of Reversible Photomechanical Crystals Based on 9-Anthracenecarboxylic Acid

Thomas J. Gately[(1)], Watit Sontising[(1)], Connor J. Easley[(1)], Imadul Islam[(2)], Rabih O. Al-Kaysi[(2)]*, Gregory J. O. Beran[(1)]*, and Christopher J. Bardeen[(1)]*

[(1)]Department of Chemistry
University of California, Riverside
Riverside, CA 92521

[(2)]College of Science and Health Professions-3124,
King Saud bin Abdulaziz University for Health Sciences, and King Abdullah International Medical Research Center (Nanomedicine), Ministry of National Guard Health Affairs, Riyadh 11426,
(Kingdom of Saudi Arabia)

Abstract

9-anthracene carboxylic acid derivatives comprise a family of thermally reversible photomechanical molecular crystals. The photomechanical response relies on a [4+4] photodimerization followed by dissociation that occurs on timescales of seconds to minutes. A combined theoretical and experimental investigation is undertaken to better understand how chemical modification of the anthracene core influences energetics of both the isolated molecule and the crystal lattice. We use both density functional theory and dispersion-corrected Moller-Plesset perturbation theory computational methods to establish orbital energies, photodimerization reaction energies, and lattice energies for a set of substituted 9-anthracene carboxylic acid molecules. The calculations reveal that steric interactions play a dominant role in the ability to form photodimers and indicate an energetic threshold of 80-90 kJ/mole for the dimerization reaction. Examination of intermolecular bonding in a subset of fluorinated **9ACs** revealed the

absence of H…F intermolecular bond formation and energy differences that can explain observed trends in the dissociation kinetics and mechanical reset times. Fluorescence recovery after photobleaching experiments show that the photodimer dissociation kinetics depend on the amount of initial photodimer, preventing a straightforward correlation between halogen atom substitution and dissociation rates using the Bell-Evans-Polanyi principle. The results clarify how molecular structure affects intermolecular interactions and photoreactivity in this family of molecular crystals, but the origin of the complex photodimer dissociation dynamics remains an open question.

Introduction

Crystals composed of photoreactive molecules (photochromes) can transform light energy directly into mechanical work.[1-3] They do this by organizing the molecules so that geometrical changes associated with the geometric photoisomerization, photodimerization, or photocyclization add together in specific directions determined by the crystal axes. Various classes of both intra- and intermolecular reactions have been harnessed to generate this work. In the latter class, [2+2][4-12] and [4+4] [13-16] photodimeriztion reactions are commonly used. To realize thermally reversible (T-type) photomechanical crystals based on photodimerization, the photodimer must be sufficiently unstable so that its dissociation proceeds rapidly at room temperature. In this context, we have synthesized and studied a class of substituted 9-anthracenecarboxylic acid (**9AC**) derivatives that crystallize in a head-to-head (*hh*) geometry due to intermolecular hydrogen bonding between neighboring stacks.[17] The *hh* geometry gives rise to steric interactions between the COOH groups on cofacial molecules that destabilize the C-C bridge bonds of the photodimer and cause it to spontaneously dissociate back into the monomer pair.[18-21] This ability of the crystal to reset itself after photodimerization makes it a T-type photomechanical material that could have practical applications.

The **9AC** core provides the basis for an entire class of photomechanical molecular crystals because chemical substituents can be added to the anthracene ring in order to tune the material properties. The effects of halogen atom and methyl group substitution on the photodimerization and recovery kinetics have been investigated in two previous papers.[22, 23] One surprising result was that F-atom substitution at different carbons around the anthracene ring led to photodimer dissociation rates that varied by more than an order of magnitude, despite virtually identical crystal packing geometries. To explain this observation, we hypothesized that intermolecular H…F

interactions might affect the relative stabilities of the monomer and photodimer in the different molecular crystals.[23] If the rate of photodimer dissociation can be controlled by the F substitution pattern, this would provide a strategy to design molecular crystals with desired properties, like fast mechanical recovery times.

In this paper, we undertake a combined theoretical and experimental investigation to better understand how chemical modification of the **9AC** core influences energetics of both the isolated molecule and the crystal lattice. The goal is to determine the relative importance of local (pairwise) versus nonlocal (crystal) interactions in determining the photochemical reactivity of monomer pairs and the stability of photodimers. We examine a large set of substituted **9AC** molecules (Scheme 1) using both density functional theory (DFT) and dispersion-corrected Moller-Plesset perturbation theory (MP2D)[24] computational methods to establish orbital energies, photodimerization reaction energies, and lattice energies. The Bell-Evans-Polanyi (BEP) principle provides a way to correlate the energy difference between a monomer pair and photodimer with the activation energy and thus the thermal dissociation rate.[25-28] These calculations reveal that steric interactions play a dominant role in the ability to form photodimers and suggest there exists an energetic threshold for the formation of the photodimer, but they fail to show any relation between enthalpy differences and observed photodimer dissociation rates. Additional kinetic experiments show that the photodimer dissociation, as measured by the recovery of the monomer fluorescence, is highly nonlinear and depends on the amount of initial photodimer created by the ultraviolet (UV) pulse. The complex reaction kinetics in the crystals prevent a straightforward correlation between halogen atom substitution and dissociation rates. This work clarifies how molecular structure affects intermolecular interactions and photoreactivity in the crystal, but the origin of the complex reaction dynamics in this class of hydrogen-bonded crystals remains unclear.

Experimental Methods

The syntheses of the **10F-9AC**, **10Methyl-9AC**, **10Cl-9AC**, **10Br-9AC**, and **10Ph-9AC** were previously reported.[22] The syntheses of **2F-9AC**, **4F-9AC**, and **2,6diF-9AC** were described previously.[23] Detailed synthetic procedures for **4,5diF-9AC**, **2Cl-9AC**, **4Cl-9AC**, and **4,5diCl-9AC** is described in the Supporting Information. Crystal structures for all molecules except **4Cl-9AC** and **2Cl-9AC** are also given in the Supporting Information.

The measurement of the fluorescence recovery process was performed using an Olympus IX70-inverted microscope. Crystals of the compounds were placed on glass microscope slides. Large rectangular crystals were used for measurements because of their resistance to bending and deformation, preventing misalignment of the pump and probe beams. The alignment of each crystal was confirmed after UV exposure to ensure accurate fluorescence recovery data. Utilizing a pump-probe setup a 405 nm laser was used to irradiate samples for a predetermined time then probed using a less intense 405 nm beam. A Melles Griot Electronic Shutter Controller (04 ISC 850) and a custom LabView program were used to control the pump exposure. The probe spot radius of 17 μm was three times smaller than the 55 μm pump beam. The beam was modulated by a chopper at a frequency of 100 Hz. The resulting signal was obtained using a lock-in amplifier with a photomultiplier tube. To reduce probe beam exposure, intermittent blocking was performed manually during the data collection.

The interpretation of the fluorescence recovery experiments relies on the assumption that the fluorescence is linearly proportional to the monomer population. Previous experiments showed that the fluorescence of the monomer crystal originates from an excimer and is redshifted about 100 nm below the absorption edge[29], allowing us to assume that reabsorption of the fluorescence

by monomer or photodimers is negligible and these optical nonlinearities can be neglected. In the same work, it was found that the loss of fluorescence was linearly proportional to the UV photon dose, again consistent with a linear relation between the loss of monomer and loss of fluorescence. Thus the available data suggests that the fluorescence signal is a good surrogate for the monomer pair population.

Computational Methods

The geometries of gas-phase monomers, dimers, and tetramers of the **F-9AC** species and their photodimerized analogs were optimized using the BLYP[30, 31] generalized gradient approximation (GGA) density functional with the D3(BJ) dispersion correction[32, 33] and the def2-TZVP basis set.[34] Frontier orbital energies and quasi-particle gaps were then computed for gas-phase **F-9AC** monomers using single-point energies computed with the range-separated hybrid ωB97X-D density functional[35] in the aug-cc-pVTZ basis set.[36] The highest-occupied molecular orbital (HOMO) energy was equated to the negative of the ionization potential, while the lowest-unoccupied molecular orbital (LUMO) energy was the set to be the negative of the electron affinity. The ionization potentials and electron affinities were computed via the ΔSCF approach[37], taking the energy difference between the neutral species and its corresponding cation or anion. Optical gaps corresponding to vertical excitations were computed via time-dependent density functional theory (TDDFT) using the same ωB97X-D/aug-cc-pVTZ model in implicit cyclohexane polarizable continuum solvent.[38]

The energetics of anthracene photodimerization are notoriously difficult to model, and the results from many common density functionals are both quantitatively and qualitatively incorrect.[24, 39] Therefore, the **F-9AC** species and their gas-phase photodimerization reactions in

dimer and tetramer clusters were computed with dispersion-corrected second-order Møller-Plesset perturbation theory (MP2D)[24], which has been shown to model anthracene photodimerization energetics to within a few kcal/mol of coupled cluster theory benchmarks. The MP2D calculations were extrapolated to the complete basis set (CBS) limit by combining Hartree-Fock/aug-cc-pVQZ results with correlation energies extrapolated from the aug-cc-pVTZ and aug-cc-pVQZ basis sets.[40] These large basis sets were chosen to help converge the energetics and to reduce basis set superposition error. Because the counterpoise correction[41] is ill-defined for intramolecular interactions, it was not employed here to avoid inconsistencies between the description of the intermolecular π-stacking interactions in the reactants versus the intramolecular interactions in the photodimer product. The TDDFT calculations were performed using Gaussian 16 RevC.01.[42] All other gas-phase calculations were performed using PSI4[43], employing density fitting algorithms and the default auxiliary basis sets throughout. The MP2D dispersion correction is available in the current developmental version of PSI4 or can be downloaded as a stand-alone library for use with any MP2 implementation.

Solid-state calculations on **F-9AC** crystals were performed using the B86bPBE generalized gradient approximation functional[44, 45] and the exchange-hole dipole moment (XDM) dispersion correction[46] using QuantumEspresso 6.4.1[47, 48], a 50 Ry planewave cutoff, and Monkhorst-Pack grids with a k-point density of ~0.04 A^{-1}. Core electrons were treated via the projector augmented wave (PAW) approach using PAW potentials for H, C, and F generated with A. Dal Corso's Atomic code v6.1. Experimental crystal structures were relaxed with lattice parameters held fixed at their experimental values. For higher accuracy and consistency with the gas-phase calculations, the single-point crystal lattice energies of the optimized structures were then refined by extracting the key reactive tetramer (two π-stacked pairs of hydrogen bonded dimers), then replacing the DFT

energy of that gas-phase tetramer with the corresponding MP2D energy. This approximation is essentially the same as the monomer-correction approach[49] that has proved extremely useful in a number of other organic crystals,[49-51] including the related 9-tertbutyl anthracene ester.[52] The approximation amounts to describing the most important local interactions—those within the key reactive tetramer—with MP2D, while the longer-range contributions arising from the interaction of that tetramer with the surrounding crystal lattice are modeled with periodic DFT. For further insight, the lattice energies were decomposed into contributions arising from within the central tetramer, between the tetramer and the rest of the crystal, and the energy required to distort the monomer from its optimal gas-phase geometry to the crystalline conformation. The interactions in the tetramer were further decomposed into all possible pairwise interactions (consisting of hydrogen bonded pairs, π-stacked pairs, and "diagonal" pairs) plus the residual non-pairwise-additive "many-body" contribution.

Results and Discussion

A. Effect of Halogen Substitution on Molecular Electronic Properties

We first wanted to understand how chemical substitution affects the photophysical properties of individual molecules. In the simplest limit, electron withdrawing groups are expected to lower the HOMO and LUMO energies. From a practical standpoint, this should make the molecule more difficult to oxidize and increase its stability, since reaction with ambient O_2 molecules at the C10 and C9 carbons is a major side reaction for photoexcited anthracene molecules leading to 9,10-endoperoxyanthracene derivative that can rearrange to give anthraquinones.[53, 54] Figure 1 shows the calculated gas-phase HOMO/LUMO energy level shifts for the various **9AC** derivatives in Scheme 1. As expected, the addition of electron-withdrawing atoms like Cl and F systematically

lowers both orbital energies. Surprisingly, Cl substitution seems to have a slightly larger effect, even though it is less electronegative than F. But although the individual orbitals shift by as much as 0.5 eV upon halogen substitution, the HOMO/LUMO shifts tend to offset each other, with the net result that the HOMO/LUMO gap does not change by more than 0.2 eV.

The stability of the HOMO-LUMO gap with respect to chemical substitution is mirrored by the calculated optical gap. Figure 2a shows representative absorption spectra for **9AC** and some fluorinated derivatives. All derivatives retain the characteristic anthracene vibronic lineshape, suggesting that the S_0-S_1 transition has a similar electronic character in all of them. In Figure 2b we plot the experimental S_0-S_1 transition energies in cyclohexane, as well calculated S_0-S_1 optical energies in implicit cyclohexane solvent for **9AC**, **10F-9AC**, **2F-9AC**, **4F-9AC**, **2,6diF-9AC** and **4,5diF-9AC**. Fluorine substitution causes the measured absorption peak to shift by up to 0.1 eV, while the calculated S_0-S_1 gaps show more scatter but the same magnitude of variation. The calculated S_0-S_1 energies are consistently about 0.1 eV greater than the experimental energies, which is within the typical accuracy for TDDFT calculations.[55, 56] The experimental and calculated S_0-S_1 energies and absorption lineshapes are consistent with previous work showing that halogen atom substitution on the anthracene ring can shift the absolute HOMO/LUMO positions but has little effect on the molecule's optical properties.[57, 58]

B. Effect of Halogen Substitution on Dimer Energetics

In solution, anthracene carboxylic acids photodimerization typically favors the head-to-tail (*ht*) conformation.[59, 60] In the crystal form, hydrogen bonds between COOH groups on opposing molecules lock the molecules in the *hh* conformation along the one-dimensional stacks. Gas-phase MP2D calculations comparing the *hh* and *ht* arrangements of the photodimer (Table 1) show that

the *hh* photodimer geometry is generally ~32-35 kJ/mol less stable than the *ht* one due to the steric clash introduced by having the two COOH groups on the same side in the *hh* geometry. In contrast, the energy differences between the *hh* and *ht* geometries of the unreacted gas-phase dimers are only ~3-7 kJ/mol. Taken together, this means that the reaction energies ΔE_{rxn} = *E(photodimer) – E(unreacted)* for the *hh* dimerization are considerably more endothermic than the *ht* ones (Table 1). This explains why the photodimerization is so easily reversible in the **9AC** crystals at room temperature, since only the highly endothermic *hh* dimerization can occur in the crystalline state. Most of the fluorine substitutions considered impact the energy difference between the *ht* and *hh* photodimers minimally (*i.e.* by 2—3 kJ/mol), except for **10F-9AC** where the *hh* photodimer is actually 14 kJ/mol more stable than the *ht* photodimer. In this case, the unfavorable electrostatic repulsion between the COOH and/or F groups on the adjacent anthracene units mean that neither the *ht* nor *hh* arrangement is particularly favored. Moreover, both *hh* and *ht* configurations of **10F-9AC** exhibit more endothermic gas-phase photodimerization energies ΔE_{rxn} than any of the other derivatives (Table 1), according to these calculations.

Next, we consider the gas-phase MP2D *hh* photodimerization energies ΔE_{rxn}*(hh)* across a broader set of **9AC** derivatives in Table 2, including both ones that have been tested experimentally and other hypothetical mono-halogenated **9AC** derivatives. The crystal photoreactivity was determined by direct observation of the loss of monomer fluorescence and mechanical changes under 405 nm irradiation. Figure 3 plots ΔE_{rxn} for several **9AC** derivatives and indicates whether they exhibit experimental reactivity in the crystal form. The photodimerization of these **9AC** derivatives is consistently endothermic, and there seems to be a ΔE_{rxn} threshold at around 90 kJ/mol, above which dimer formation is prevented. These higher-energy photodimerization reactions have larger substituents located at the 10-position that cannot avoid interacting with each

other. Among the hypothetical cases, dimerization appears energetically feasible for any fluorine, chlorine, or bromine mono-halogenation at the 2, 3, or 4 positions, with dimerization reaction energies 62--73 kJ/mol. Mono-fluorination at the 1 position also exhibits a dimerization energy comparable to that of **10F-9AC**, while reactions involving larger Cl and Br substituents in the 1 position are unlikely, since they have ΔE_{rxn} of 100 kJ/mol or more. Similar to the **10X-9AC** derivatives, these highly endothermic reaction energies stem from steric clashes between the COOH and the halogen groups. It should be noted that ΔE_{rxn} is the difference between ground state isomers and thus in principle provides no information about the excited state potential energy surface that determines the photodimerization yield. However, we suspect that it indicates the degree of steric interference within the dimer, which is an important factor in determining whether photodimerization proceed on the excited state. This correlation with sterics probably explains why it correlates with photoreactivity as well.

C. Effect of Halogen Substitution on Tetramer and Crystal Energetics

In order to test our hypothesis that intermolecular bonding plays an important role in the reaction kinetics, we had to examine larger systems. The metastable nature the **9AC** photodimer has prevented experimental characterization of its neat crystal structure, although solvates have been investigated.[61] Without knowledge of the photodimer crystal structures, the computational modeling instead focused on a gas-phase tetramer cluster model in which two pairs of hydrogen bonded monomers could be photodimerized, as illustrated in Figure 4. These more expensive calculations were performed on a subset of the experimentally investigated molecules in Section B. These clusters were extracted from the unreacted monomer crystal, and then either one or both of the monomer pairs in the tetramer were converted to photodimers and the tetramer structure was

relaxed. The photodimerization reaction energy in the tetramer is moderately less favorable than in the dimer. As shown in Table 3, the first dimerization within the tetramer is ~11 kJ/mol more endothermic on average, while the second one is ~19 kJ/mol more endothermic. These higher reaction energies reflect the geometric constraints associated with preserving the COOH hydrogen bonds between the stacks. Nevertheless, the qualitative trends in the reaction energies for the different F substitution patterns in the tetramer remain similar to those in the isolated dimer. **4F-9AC** again exhibits the lowest ΔE_{rxn}, while **10F-9AC** has largest ΔE_{rxn} and thus would be predicted to be the least stable photodimer.

The similarities of the dimer and tetramer cluster results motivated us to examine the energetics of the monomer crystal lattice in more detail. The goal was to look for any variations in the intermolecular forces that arise from fluorine substitution. The crystal lattice energies are analyzed by decomposing them into contributions arising from (i) distortion of the monomer from its gas-phase to crystalline conformation, (ii) the interaction energy within the key tetramer unit, and (iii) the interaction of that tetramer with the rest of the crystal lattice. As shown in Figure 5a, the intermolecular interactions within the tetramer represent the strongest contribution to the lattice energy, but the interactions between the tetramer and the lattice energy are almost as large.

One might anticipate the fluorine substitution could create additional hydrogen bonding between tetramer units that would increase the lattice energy. However, the data provides little evidence for the role of intermolecular H…F bonding. With typical H...F distances of 2.3-2.5 Angstroms, the intermolecular H…F bonds are relatively weak. If such H…F bonds were important, they would impact the interaction energy between the tetramer and the rest of the lattice, but these interactions vary by only a few kJ/mol across most of the derivatives (Figure 5a). The only notable exception occurs for **2,6-diF-9AC**, for which F…F repulsion actually weakens these

interactions by about ~10 kJ/mol relative to the other derivatives. Fluorine substitution has only minor impacts on the other energy contributions as well. For example, the interactions within the tetramer vary by only ~2 kJ/mol across the derivatives, and the differences among the monomer distortion energies are similarly small (with **2,6-diF-9AC** again being a moderate exception). In the end, the total lattice energies for all derivatives lie in the 141-146 kJ/mol range, except for **2,6-diF-9AC** at 131 kJ/mol (due to the aforementioned F…F repulsion and larger distortion energy penalties).

It seemed surprising the F substitution had such small impacts on the tetramer energies, since it is known that halogenation can impact pi-stacking interactions appreciably.[62] Figure 5b further decomposes the intermolecular interactions within the key tetramer into the sum of the two pairwise hydrogen bond interactions, the sum of the two π-stacking energies, the two pairs of "diagonal" interactions, and the residual many-body contribution arising from the beyond-pairwise interactions within the tetramer. As expected, we do observe that fluorination systematically increases the strength of the π-stacking interactions by up to 5 kJ/mol, and the di-fluorinated species stacks are stabilized more than the mono-fluorinated ones. However, the other interactions vary less systematically with fluorine substitution, and the net effect is that the improved π-stacking energetics are largely cancelled out in the tetramer as a whole. This conclusion is consistent with the fact that most of the derivatives exhibit almost identical crystal packing (except for **10F-9AC**). Overall, these results highlight how the details of crystal packing stability on the whole can defy simple intuitive logic derived from knowledge of individual pairwise intermolecular interactions.

Given the weak effect of F-substitution on the crystal energetics, it is perhaps not surprising that we find no strong correlation between the energetics and the dimer dissociation rate.

According to the BEP principle, ΔE_{rxn} should also correlate with the dissociation rate through its activation energy. In Figure 6a, we plot the dissociation half lives ($\tau_{1/2}$ from reference [23])versus the dimer ΔE_{rxn} for molecules **9AC**, **10F-9AC**, **2F-9AC**, **4F-9AC**, and **2,6diF-9AC**. Unlike Figure 3, there is no obvious correlation. The inclusion of dimer-dimer interactions by using a tetramer cluster does not change this situation, as shown in Figure 6b. In both cases, the largest predicted *hh* photodimerization energy ΔE_{rxn} in Table 1 is found for **10F-9AC**, while the smallest one occurs for **4F-9AC**. If the dimer→monomer pair reactions of the different derivatives have similar transition state structures, the BEP principle would predict the **10F-9AC** dimer to have the fastest dissociation rate and **4F-9AC** to have the slowest rate. This is precisely the opposite of what is observed experimentally.

D. Nonlinear Photodimer Dissociation Kinetics

The absence of a correlation between ΔE_{rxn} and the photodimer lifetimes in Figure 6 suggests that the BEP principle cannot be naively applied to this class of reactions. One assumption of the BEP model is that the Arrhenius prefactors and transition state structures are similar within the family of compounds under study. While this assumption seems reasonable for the **9AC**s, it may be that the transition state is much more sensitive to the surrounding crystal environment than the minimum energy monomer and dimer configurations. A second possibility is that the accurate calculation of the photodimer energies requires taking the full crystal lattice into account, rather than isolated clusters. However, there is no hint from the monomer calculations that the inclusion of such terms would shift the relative energies by more than a few kJ/mol. Rather than focusing on energetics, a third explanation centers on the possibility that the bulk photodimer dissociation kinetics are more complicated than the simple two-state model that underlies the BEP principle.

In the ideal case, the photodimerization can be described by a simple two-state model subject to well-defined forward and backward first-order rate constants that are independent of concentration. This assumption is usually valid in dilute solution, where the molecules react independently in a homogeneous environment. But in a crystal, where the reacting molecules are in intimate contact, the surrounding can change as the fraction of dimers evolves, leading to a time-dependent rate that changes as the reaction progresses.[63-65] In this limit, a single rate cannot describe the process and it is no longer possible to make a straightforward connection between equilibrium energies and dynamics. One hallmark of such nonlinear kinetics is their dependence on initial concentrations. Recent studies on the kinetics of the dimer dissociation in **4F-9AC** crystals showed strong deviations from first-order exponential behavior, where a larger initial photodimer concentration slowed down the dissociation reaction and the recovery of the monomer fluorescence signal.[29] The recovery was also sensitive to the presence of a 100× weaker probe beam that could stall the monomer recovery. We interpreted these concentration-dependent decays as evidence of cooperative dynamics, perhaps related to nucleation.

To determine whether the linear kinetic model is valid for the other **9AC** derivatives, we measured the kinetics of monomer recovery using a fluorescence recovery after photobleaching (FRAP) experiment. We were careful to only use an intermittent probe technique so the fluorescence detection did not perturb the recovery and found concentration-dependent kinetics in all of them to varying degrees. Figure 7 compares the high and low bleach (initial photodimer concentration) recovery curves for molecules **9AC**, **10F-9AC**, **2F-9AC**, **4F-9AC**, and **2,6diF-9AC**. All exhibit slower decays for large bleach depths (high initial photodimer conversion), with the effect being most pronounced for **9AC** and least pronounced for **2,6diF-9AC** and **10F-9AC**. Note that **9AC** can be grown in two different polymorphs, monoclinic and triclinic.[22] This

different symmetry arises from the slightly different arrangement of the one-dimensional stacks along the *b*-axis, as detailed in the Supporting Information. The same nonlinear behavior was seen in both polymorphs (Supporting Information), providing additional experimental evidence that subtle changes in stack orientation do not strongly affect the dissociation kinetics.

As in our previous paper[23], we can to parameterize the data in Figure 7 by extracting $\tau_{1/2}$, the time required for the fluorescence recovery to achieve 50% of its pre-bleach value. These values are summarized in Table 4. For low bleach depths (low initial photodimer concentrations), the $\tau_{1/2}$ recovery times are similar for all molecules except **10F-9AC**, as shown in Figure 8a. For deeper bleaches, Figure 8b shows how the $\tau_{1/2}$ times diverge by a factor of 10. From Figure 8a, it appears that any discrepancy between the $\tau_{1/2}$ values for different compounds is magnified when large (>20%) photodimer conversions are measured. The similarity of the low conversion recovery rates among the different compounds suggests that local energetic considerations, predicted by theory to be similar, are controlling the dissociation of dilute dimers. At higher concentrations, however, it is possible that many-body effects become important, and these cannot be identified by the dimer and tetramer level of theory employed here. We note that **10F-9AC** continues to be an outlier, even for low conversions.

In an earlier paper, we did not realize that the bleach depth and the presence of the probe beam could have a significant effect on the recovery dynamics.[23] Although the qualitative conclusions from that work are still valid, the quantitative comparison of recovery times is considerably more complex than we appreciated at that time. The origin of the variable dissociation behavior among the **9AC** derivatives remains a mystery. The kinetic behavior of a photodimer surrounded by monomer pairs must be quite different from that of one surrounded by other photodimers. It is possible that the strong intermolecular hydrogen-bond interactions in the **9AC** family make these

compounds more susceptible to such cooperative phenomena. It is also possible that this kinetic phenomenon is affected by presence of crystal defects, which could vary between derivatives. One clue to the origin of the nonlinear kinetics is that **2,6-diF-9AC** appears to be the least susceptible to the cooperative effects, with the recovery times at both high and low bleach depths being quite similar. This relative insensitivity is consistent with its weaker intermolecular interactions as predicted by calculations shown in Figure 5a. Weaker interactions can allow the dissociation kinetics to be more effectively decoupled from neighboring sites and lead to more standard first-order kinetics. Even though a direct connection to the rate is not possible because there is no single, well-defined Arrhenius rate, this observation provides a starting point for future investigations.

Conclusion

To summarize, extensive calculations of the crystal energetics and kinetic measurements for a series of **9AC** derivatives have provided insight into the reaction dynamics of this class of T-type photomechanical crystals. The important role of steric interactions and *hh* packing in determining the ability to create a metastable photodimer in the crystal was confirmed and clarified. Careful examination of intermolecular bonding in a subset of fluorinated **9AC**s revealed an absence of H…F intermolecular bond formation and a lack of clear energy differences that could explain observed trends in the dissociation kinetics and mechanical reset times. Instead, it appears that differences between molecules reflect variations in cooperative phenomena that give rise to highly nonlinear (concentration dependent) kinetics. It is possible that such kinetics are especially pronounced in the **9AC** series due to the presence of strong intermolecular COOH bonds. With a more detailed understanding, it may be possible to design molecular structures that

optimize intermolecular interactions to amplify or suppress such collective phenomena and create light-responsive crystals with novel properties.

Acknowledgements

C.J.B. acknowledges support from the National Science Foundation grant DMR-1810514 and by the MURI on Photomechanical Material Systems (ONR N00014-18-1-2624). R.O.K. acknowledges the support of KSAU-HS/KAIMRC through grant RC10/104. G.B. gratefully acknowledges funding for this work from the National Science Foundation (CHE-1955554) and supercomputer time from XSEDE (TG-CHE110064). T.J.G. gratefully acknowledges the support received from the support and scholarships received from the U.S. Air Force.

References

1. Kim, T.; Zhu, L.; Al-Kaysi, R. O.; Bardeen, C. J., Organic photomechanical materials. *ChemPhysChem* **2014,** *15*, 400-414.
2. Naumov, P.; Chizhik, S.; Panda, M. K.; Nath, N. K.; Boldyreva, E., Mechanically Responsive Molecular Crystals. *Chem. Rev.* **2015,** *115*, 12440-12490.
3. White, T. J., *Photomechanical Materials, Composites, and Systems*. 1 ed.; Wiley: Hoboken, New Jersey, 2017.
4. Naumov, P.; Kowalik, J.; Solntsev, K. M.; Baldridge, A.; Moon, J.-S.; Kranz, C.; Tolbert, L. M., Topochemistry and photomechanical effects in crystals of green fluorescent protein-like chromophores: effects of hydrogen bonding and crystal packing. *J. Am. Chem. Soc.* **2010,** *132*, 5845-5857.
5. Kim, T.; Zhu, L.; Mueller, L. J.; Bardeen, C. J., Dependence of the solid-state photomechanical response of 4-chlorocinnamic acid on crystal shape and size. *CrystEngComm* **2012,** *14*, 7792-7799.
6. Medishetty, R.; Husain, A.; Bai, Z.; Runceviski, T.; Dinnebier, R. E.; Naumov, P.; Vittal, J. J., Single crystals popping under UV light: a photosalient effect triggered by a [2+2] cycloaddition reaction. *Angew. Chem. Int. Ed.* **2014,** *53*, 5907-5911.
7. Medishetty, R.; Sahoo, S. C.; Mulijanto, C. E.; Naumov, P.; Vittal, J. J., Photosalient Behavior of Photoreactive Crystals. *Chem. Mater.* **2015,** *27*, 1821-1829.
8. Wang, H.; Chen, P.; Wu, Z.; Zhao, J.; Sun, J.; Lu, R., Bending, Curling, Rolling, and Salient Behavior of Molecular Crystals Driven by [2+2] Cycloaddition of a Styrylbenzoxazole Derivative. *Angew. Chem. Int. Ed.* **2017,** *56*, 9463 –9467.
9. Samanta, R.; Ghosh, S.; Devarapalli, R.; Reddy, C. M., Visible Light Mediated Photopolymerization in Single Crystals: Photomechanical Bending and Thermomechanical Unbending. *Chem. Mater.* **2018,** *30*, 577−581.
10. Samanta, R.; Kitagawa, D.; Mondal, A.; Bhattacharya, M.; Annadhasan, M.; Mondal, S.; Chandrasekar, R.; Kobatake, S.; Reddy, C. M., Mechanical Actuation and Patterning of Rewritable Crystalline Monomer−Polymer Heterostructures via Topochemical Polymerization in a Dual-Responsive Photochromic Organic Material. *ACS Appl. Mater.* **2020,** *12*, 16856−16863.
11. Yadava, K.; Vittal, J. J., Photosalient Behavior of Photoreactive Zn(II) Complexes. *Cryst. Growth De.* **2019,** *19*, 2542-2547.
12. Tong, F.; Xu, W.; Guo, T.; Lui, B. F.; Hayward, R. C.; Palffy-Muhoray, P.; Al-Kaysi, R. O.; Bardeen, C. J., Photomechanical molecular crystals and nanowire assemblies based on the [2+2] photodimerization of a phenylbutadiene derivative. *J. Mater. Chem. C* **2020,** *8*, 5036-5044.
13. Al-Kaysi, R. O.; Muller, A. M.; Bardeen, C. J., Photochemically driven shape changes of crystalline organic nanorods. *J. Am. Chem. Soc.* **2006,** *128*, 15938-15939.
14. Koshima, H.; Uchimoto, H.; Taniguchi, T.; Nakamura, J.; Asahi, T.; Asahi, T., Mechanical motion of molecular crystals induced by [4 + 4] photodimerisation. *Cryst. Eng. Comm.* **2016,** *18*, 7305-7310.
15. Salzillo, T.; Brillante, A., Commenting on the Photoreactions of Anthracene Derivatives in the Solid Stte. *Cryst. Eng. Comm.* **2019,** *21*, 3127–3136.

16. Tong, F.; Bardeen, C. J.; Al-Kaysi, R. O., Photomechanical Crystals Made from Anthracene Derivatives. In *Mechanically Responsive Materials for Soft Robotics*, Koshima, H., Ed. Wiley-VCH: Weinheim, Germany, 2020.
17. More, R.; Scholz, M.; Busse, G.; Busse, L.; Paulmann, C.; Tolkiehn, M.; Techert, S., Hydrogen Bond Dynamics in Crystalline b-9-Anthracene Carboxylic Acid -- a Combined Crystallographic and Spectroscopic Study. *Phys. Chem. Chem. Phys.* **2012,** *14*, 10187-10195.
18. Ito, Y.; Fujita, H., Formation of an unstable photodimer from 9-anthracenecarboxylic acid in the solid state. *J. Org. Chem.* **1996,** *61*, 5677-5680.
19. Al-Kaysi, R. O.; Bardeen, C. J., Reversible photoinduced shape changes of crystalline organic nanorods. *Adv. Mater.* **2007,** *19*, 1276-1280.
20. Zhu, L.; Al-Kaysi, R. O.; Bardeen, C. J., Reversible photoinduced twisting of molecular crystal microribbons. *J. Am. Chem. Soc.* **2011,** *133*, 12569-12575.
21. More, R.; Busse, G.; Hallmann, J.; Paulmann, C.; Scholz, M.; Techert, S., Photodimerization of crystalline 9-anthracenecarboxylic acid: a nontopotactic autocatalytic transformation. *J. Phys. Chem. C* **2010,** *114*, 4142-4148.
22. Zhu, L.; Al-Kaysi, R. O.; Dillon, R. J.; Tham, F. S.; Bardeen, C. J., Crystal structures and photophysical properties of 9-anthracene carboxylic acid derivatives for photomechanical applications. *Cryst. Growth Des.* **2011,** *11*, 4975-4983.
23. Zhu, L.; Tong, F.; Salinas, C.; Al-Muhanna, M. K.; Tham, F. S.; Kisailus, D.; Al-Kaysi, R. O.; Bardeen, C. J., Improved Solid-State Photomechanical Materials by Fluorine Substitution of 9-Anthracene Carboxylic Acid. *Chem. Mater.* **2014,** *26*, 6007–6015.
24. Řezáč, J.; Greenwell, C.; Beran, G. J. O., Accurate Noncovalent Interactions via Dispersion-Corrected Second-Order Møller−Plesset Perturbation Theory. *J. Chem. Theory Comput.* **2018,** *14*, 4711-4721.
25. Bell, R. P., The theory of reactions involving proton transfers. *Proc. Royal. Soc. A* **1936,** *154*, 414-429.
26. Evans, M. G.; Polanyi, M., Inertia and driving force of chemical reactions. *Trans. Faraday Soc.* **1938,** *34*, 11-24.
27. Pla, P.; Wang, Y.; Alcami, M., When is the Bell–Evans–Polanyi principle fulfilled in Diels–Alder reactions of fullerenes?†. *Phys. Chem. Chem. Phys.* **2020,** *22*, 8846-8852.
28. Chen, Y.; Chang, K.-H.; Meng, F.-Y.; Tseng, S.-M.; Chou, P.-T., Broadening the Horizon of the Bell–Evans–Polanyi Principle towards Optically Triggered Structure Planarization. *Angew. Chem. Int. Ed.* **2021,** *60*, 7205–7212.
29. Easley, C. J.; Tong, F.; Dong, X.; Al-Kaysi, R. O.; Bardeen, C. J., Using light intensity to control reaction kinetics and reversibility in photomechanical crystals. *Chem. Sci.* **2020,** *11*, 9852–9862.
30. Becke, A. D., Density-fnnctional exchange-energy approximation with correct asymptotic behavior. *Phys. Rev. A* **1988,** *38*, 3098-3100.
31. Lee, C.; Yang, W.; Parr, R. G., Development of the Colic-Salvetti correlation-energy formula into a functional of the electron density. *Phys. Rev. B* **1988,** *37*, 785-789.
32. Grimme, S.; Antony, J.; Ehrlich, S.; Krieg, H., A consistent and accurate ab initio parametrization of density functional dispersion correction (DFT-D) for the 94 elements H-Pu. *J. Chem. Phys.* **2010,** *132*, 154104.
33. Grimme, S.; Ehrlich, S.; Goerigk, L., Effect of the Damping Function in Dispersion Corrected Density Functional Theory. *J. Comp. Chem.* **2011,** *32*, 1456-1465.

34. Weigenda, F.; Ahlrichs, R., Balanced basis sets of split valence, triple zeta valence and quadruple zeta valence quality for H to Rn: Design and assessment of accuracy. *Phys. Chem. Chem. Phys.* **2005,** *7*, 3297-3305.
35. Chai, J.-D.; Head-Gordon, M., Systematic optimization of long-range corrected hybrid density functionals. *J. Chem. Phys.* **2008,** *128*, 084106.
36. Jr., T. H. D., Gaussian basis sets for use in correlated molecular calculations. I. The atoms boron through neon and hydrogen. *J. Chem. Phys.* **1989,** *90*, 1007-1023.
37. Ziegler, T.; Rauk, A.; Baerends, E. J., On the calculation of multiplet energies by the Hartree-Fock-Slater method. *Theor. Chim. Acta* **1977,** *43*, 261–271.
38. Scalmani, G.; Frisch, M. J., Continuous surface charge polarizable continuum models of solvation. I. General formalism. *J. Chem. Phys.* **2010,** *132*, 114110.
39. Grimme, S.; Diedrich, C.; Korth, M., The Importance of Inter- and Intramolecular van der Waals Interactions in Organic Reactions: the Dimerization of Anthracene Revisited. *Angew. Chem. Int. Ed.* **2006,** *45*, 625-629.
40. Helgaker, T.; Klopper, W.; Koch, H.; Noga, J., Basis-set convergence of correlated calculations on water. *J. Chem. Phys.* **1997,** *106*, 9639-9646.
41. Boys, S. F.; Bernardi, F., The calculation of small molecular interactions by the differences of separate total energies. Some procedures with reduced errors. *Molec. Phys.* **1970,** *19*, 553-566.
42. M. J. Frisch, G. W. T., H. B. Schlegel, G. E. Scuseria, M. A. Robb, J. R. Cheeseman, G. Scalmani, V. Barone, G. A. Petersson, H. Nakatsuji, X. Li, M. Caricato, A. V. Marenich, J. Bloino, B. G. Janesko, R. Gomperts, B. Mennucci, H. P. Hratchian, J. V. Ortiz, A. F. Izmaylov, J. L. Sonnenberg, D. Williams-Young, F. Ding, F. Lipparini, F. Egidi, J. Goings, B. Peng, A. Petrone, T. Henderson, D. Ranasinghe, V. G. Zakrzewski, J. Gao, N. Rega, G. Zheng, W. Liang, M. Hada, M. Ehara, K. Toyota, R. Fukuda, J. Hasegawa, M. Ishida, T. Nakajima, Y. Honda, O. Kitao, H. Nakai, T. Vreven, K. Throssell, J. A. Montgomery, Jr., J. E. Peralta, F. Ogliaro, M. J. Bearpark, J. J. Heyd, E. N. Brothers, K. N. Kudin, V. N. Staroverov, T. A. Keith, R. Kobayashi, J. Normand, K. Raghavachari, A. P. Rendell, J. C. Burant, S. S. Iyengar, J. Tomasi, M. Cossi, J. M. Millam, M. Klene, C. Adamo, R. Cammi, J. W. Ochterski, R. L. Martin, K. Morokuma, O. Farkas, J. B. Foresman, and D. J. Fox *Gaussian 16, Revision C.01*, Gaussian, Inc: Wallingford CT, 2016.
43. Parrish, R. M.; Burns, L. A.; Smith, D. G. A.; Simmonett, A. C.; DePrince, A. E.; Hohenstein, E. G.; Bozkaya, U. u.; Sokolov, A. Y.; Remigio, R. D.; Richard, R. M.; Gonthier, J. r. m. F.; James, A. M.; McAlexander, H. R.; Kumar, A.; Saitow, M.; Wang, X.; Pritchard, B. P.; Verma, P.; Schaefer, H. F.; Patkowski, K.; King, R. A.; Valeev, E. F.; Evangelista, F. A.; Turney, J. M.; Crawford, T. D.; Sherrill, C. D., PSI4 1.1: An Open-Source Electronic Structure Program Emphasizing Automation, Advanced Libraries, and Interoperability. *J. Chem. Theory Comput.* **2017,** *13*, 3185−3197.
44. Becke, A. D., On the large-gradient behavior of the density functional exchange energy. *J. Chem. Phys.* **1986,** *85*, 7184-7187.
45. Perdew, J. P.; Burke, K.; Ernzerhof, M., Generalized Gradient Approximation Made Simple. *Phys. Rev. Lett.* **1996,** *77*, 3865-3868.
46. Otero-de-la-Roza, A.; Johnson, E. R., Van der Waals interactions in solids using the exchange-hole dipole moment model. *J. Chem. Phys.* **2012,** *136*, 174109.
47. Giannozzi, P.; Baroni, S.; Bonini, N.; Calandra, M.; Car, R.; Cavazzoni, C.; Ceresoli, D.; Chiarotti, G. L.; Cococcioni, M.; Dabo, I., QUANTUM ESPRESSO: a modular and open-source

software project for quantum simulations of materials. *J. Phys.: Condens. Matter* **2009,** *21*, 395502.
48. Giannozzi, P.; Andreussi, O.; Brumme, T.; Bunau, O.; Buongiorno, M.; Nardelli; Calandra, M.; Car, R.; Cavazzoni, C.; Ceresoli, D.; Cococcioni, M.; Colonna, N.; Carnimeo, I.; Corso, A. D.; Gironcoli, S. d.; Delugas, P.; Jr, R. A. D.; Ferretti, A.; Floris, A.; Fratesi, G.; Fugallo, G.; Gebauer, R.; Gerstmann, U.; Giustino, F.; Gorni, T.; Jia, J.; Kawamura, M.; Ko, H.-Y.; Kokalj, A.; Küçükbenli, E.; Lazzeri, M.; Marsili, M.; Marzari, N.; Mauri, F.; Nguyen, N. L.; Nguyen, H.-V.; Otero-de-la-Roza, A.; Paulatto, L.; Poncé, S.; Rocca, D.; Sabatini, R.; Santra, B.; Schlipf, M.; Seitsonen, A. P.; Smogunov, A.; Timrov, I.; Thonhauser, T.; Umari, P.; Vast, N.; Wu, X.; Baroni, S., Advanced capabilities for materials modelling with Quantum ESPRESSO. *J. Phys.: Condens. Matter* **2017,** *29*, 465901.
49. Greenwell, C.; Beran, G. J. O., Inaccurate Conformational Energies Still Hinder Crystal Structure Prediction in Flexible Organic Molecules. *Cryst. Growth Des.* **2020,** *20*, 4875−4881.
50. Dracinsky, M.; Unzueta, P.; Beran, G. J. O., Improving the accuracy of solid-state nuclear magnetic resonance chemical shift prediction with a simple molecular correction. *Phys. Chem. Chem. Phys.* **2019,** *21*, 14992-15000.
51. Greenwell, C.; Beran, G. J. O., Rubrene untwisted: common density functional theory calculations overestimate its deviant tendencies. *J. Mater. Chem. C* **2021,** *9*, 2848-2857.
52. Beran, G. J. O., Solid state photodimerization of 9-tert-butyl anthracene ester produces an exceptionally metastable polymorph according to firstprinciples calculations. *Cryst. Eng. Comm.* **2019,** *21*, 758–764.
53. Stevens, B.; Perez, S. R.; Ors, J. A., Photoperoxidation of unsaturated organic molecules. XIV. O_2 ^1Dg acceptor properties and reactivity. *J. Am. Chem. Soc.* **1974,** *96*, 6846–6850.
54. Aubry, J.-M.; Pierlot, C.; Rigaudy, J.; Schmidt, R., Reversible Binding of Oxygen to Aromatic Compounds. *Acc. Chem. Res.* **2003,** *36*, 668-675.
55. Dreuw, A.; Head-Gordon, M., Single-Reference ab Initio Methods for the Calculation of Excited States of Large Molecules. *Chem. Rev.* **2005,** *105*, 4009–4037.
56. Leang, S. S.; Zahariev, F.; Gordon, M. S., Benchmarking the performance of time-dependent density functional methods. *J. Chem. Phys.* **2012,** *136*, 104101.
57. Tannaci, J. F.; Noji, M.; McBee, J.; Tilley, T. D., 9,10-Dichlorooctafluoroanthracene as a Building block for n-Type Organic Semiconductors. *J. Org. Chem.* **2007,** *72*, 5567-5573.
58. Medina, B. M.; Beljonne, D.; Egelhaaf, H. J.; Gierschner, J., Effect of Fluorination on the Electronic Structure and Optical Excitations of p-Conjugated Molecules. *J. Chem. Phys.* **2007,** *126*, 111101/1-111101/6.
59. Wolff, T.; Müller, N., Regioselective photodimerization of polar 9-substituted anthracenes in micellar solutions. *J. Photochem.* **1983,** *23*, 131-140.
60. Schutz, A.; Wolff, T., Regioselectivity in the photodimerization of 9-hydroxy-methylanthracene and 9-anthracene carboxylic acid esters in surfactant systems. *J. Photochem. Photobio. A* **1997,** *109*, 251–258.
61. Salzillo, T.; Venuti, E.; Femoni, C.; Valle, R. G. D.; Tarroni, R.; Brillante, A., Crystal Structure of the 9‑Anthracene−Carboxylic Acid Photochemical Dimer and Its Solvates by X‑ray Diffraction and Raman Microscopy. *Cryst. Growth Des.* **2017,** *17*, 3361−3370.
62. Wheeler, S. E., Understanding Substituent Effects in Noncovalent Interactions Involving Aromatic Rings. *Acc. Chem. Res.* **2013,** *46*, 1029–1038.
63. McBride, J. M.; Segmuller, B. E.; Hollingsworth, M. D.; Mills, D. E.; Weber, B. A., Mechanical Stress and Reactivity in Organic Solids. *Science* **1986,** *234*, 830-835.

64. Peachey, N. M.; Eckhardt, C. J., Energetics of Organic Solid-State Reactions: Lattice Dynamics in the 2,5-Distyrlpyrazine Photoreaction. *J. Phys. Chem.* **1993,** *97*, 10849–10856.
65. Luty, T.; Eckhardt, C. J., General Theoretical Concepts for Solid State Reactions: Quantitative Formulation of the Reaction Cavity, Steric Compression, and Reaction-Induced Stress Using an Elastic Multipole Representation of Chemical Pressure. *J. Am. Chem. Soc.* **1995,** *117*, 2441–2452.

Species	Monomer Pair ($E_{hh} - E_{ht}$) (kJ/mol)	Photodimer ($E_{hh} - E_{ht}$) (kJ/mol)	ΔE_{rxn}(hh) (kJ/mol)	ΔE_{rxn}(ht) (kJ/mol)
9AC	4.0	34.3	63.1	32.8
2F-9AC	7.3	34.8	67.0	39.4
4F-9AC	-5.0	35.1	62.3	22.2
10F-9AC	-4.7	-13.5	74.0	82.8
2,6diF-9AC	6.8	32.3	68.1	42.6
4,5diF-9AC	-3.3	32.1	60.4	25.0

Table 1: Gas-phase MP2D dimer energy differences comparing **9AC** derivatives with head-to-head (*hh*) and head-to-tail (*ht*) geometries. 1st column: *hh* versus *ht* energy difference for unreacted monomer pair; 2nd column: *hh* versus *ht* energy difference for dimerized pair; 3rd column: dimerization reaction energy for *hh* pair; 4th column: dimerization reaction energy for *ht* pair.

Molecule	X=F	X=Cl	X=Br	X=Me	X=Ph
9AC	63.1[a]	—	—	—	—
1X-9AC	76.5[c]	100.0[c]	106.2[c]	—	—
2X-9AC	67.0[a]	69.3[a]	72.8[c]	—	—
3X-9AC	66.5[c]	67.9[c]	71.7[c]	—	—
4X-9AC	62.3[a]	66.2[c]	67.1[c]	—	—
10X-9AC	74.0[a]	119.9[b]	101.7[b]	94.9[b]	204.7[b]
2,6diF-9AC	68.1[a]	—	—	—	—
4,5diF-9AC	60.4[a]	67.8[a]	—	—	—

Table 2: Gas-phase MP2D predicted dimerization energies ($\Delta E_{rxn}(hh)$) for various **9AC** compounds in the *hh* configuration, in kJ/mol. a) reactive; b) non-reactive; c) not tested.

Species	Dimer ΔE_{rxn}(hh) (kJ/mol)	Tetramer ΔE_{rxn}(hh) (kJ/mol)	$\Delta E_{rxn,2}$(hh) (kJ/mol)	$\Delta E_{rxn,avg}$(hh) (kJ/mol)
9AC	63.1	73.2	81.7	77.5
2F-9AC	67.0	79.6	83.8	81.7
4F-9AC	62.3	72.1	80.6	76.4
10F-9AC	74.0	84.3	93.4	88.9
2,6diF-9AC	68.1	79.3	88.2	83.8

Table 3: Comparison of dimerization reaction energies of fluorinated **9AC** compounds in dimer, tetramer with one pair reacted, and tetramer with both pairs reacted ($\Delta E_{rxn,2}$). The 4th column is an average of the two tetramer reaction energies.

	Shallow Bleach Recovery ($\tau_{1/2}$) (s)	Deep Bleach Recovery ($\tau_{1/2}$) (s)
9AC	7.2	174.5
2F-9AC	15.3	54.4
4F-9AC	6.5	31.5
10F-9AC	270.1	333.2
2,6diF-9AC	6.8	21.5

Table 4: The half times from shallow (~10%) and deep (~50%) fluorescence bleaches (fraction of crystal converted to the nonfluorescent photodimer) for selected **9AC** compounds.

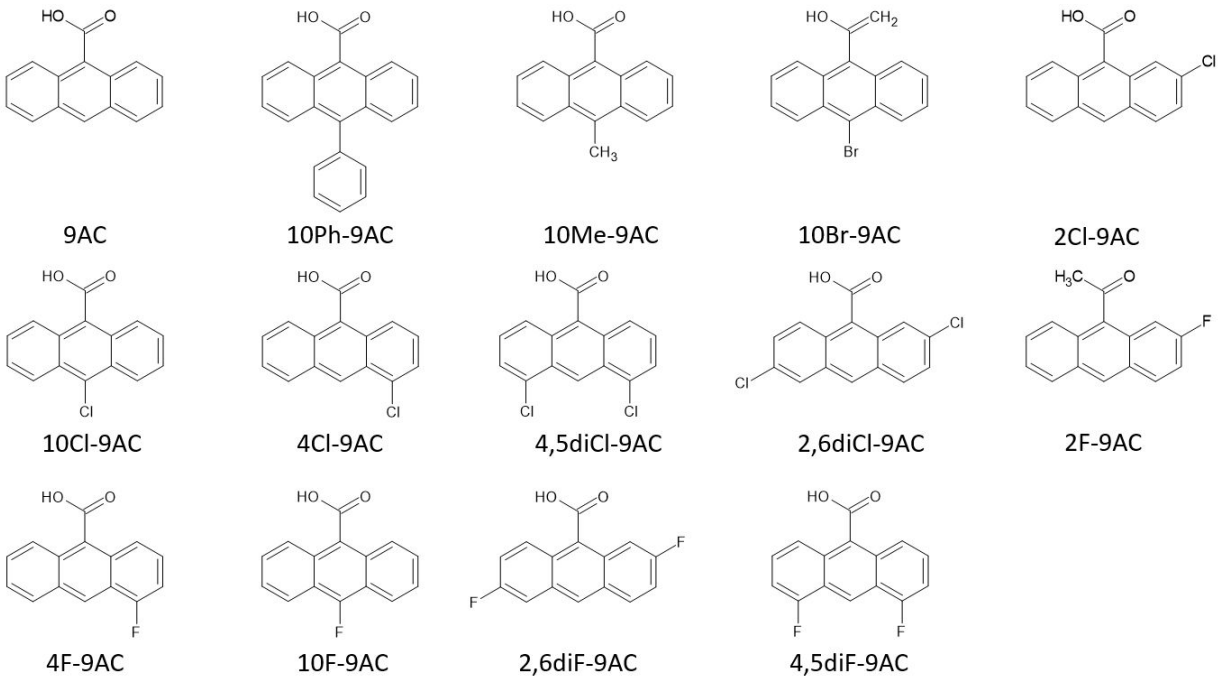

Scheme 1. 9-anthracene carboxylic acid derivatives studies in this paper, along with abbreviations use in the text.

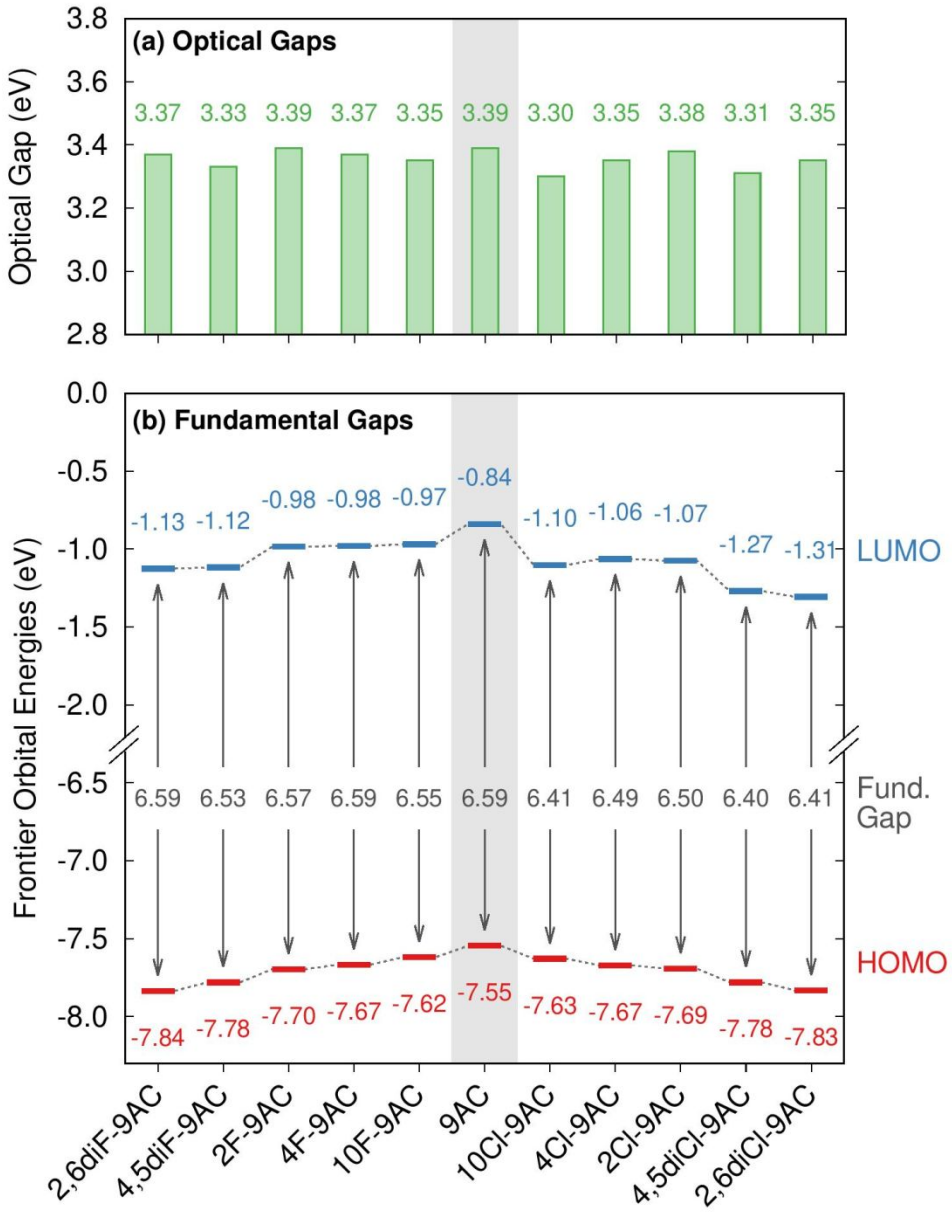

Figure 1. **a)** Optical gaps calculated for various **9AC** derivatives shown in Scheme 1. **b)** Effect of halogen substitution pattern on the HOMO/LUMO levels of **9AC**.

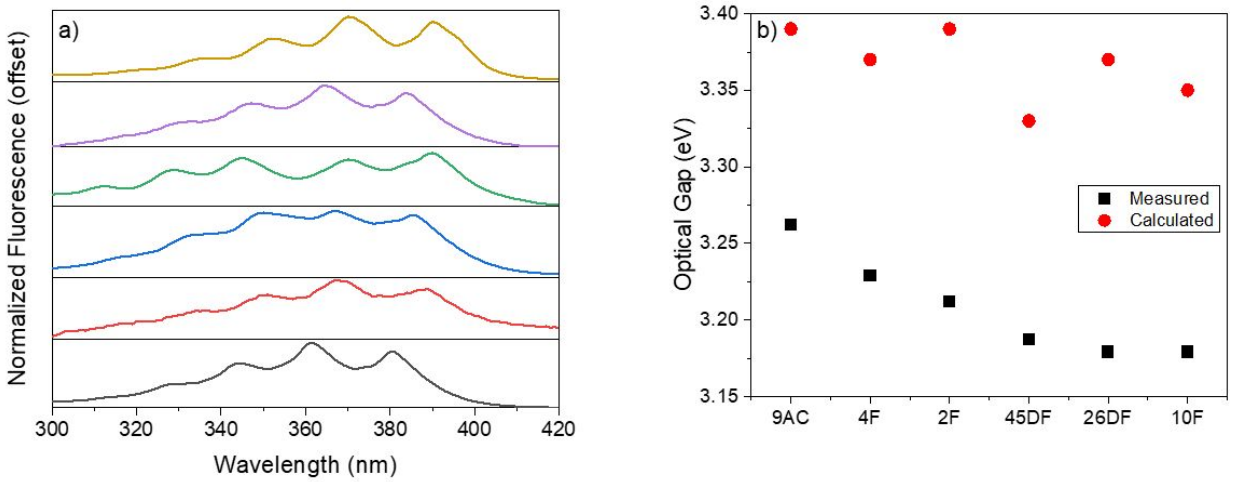

Figure 2. a) Normalized absorption spectra of **10F-9AC** (brown), **4F-9AC** (purple), **2,6diF-9AC**, **2F-9AC** (blue), **4,5diF-9AC** (red), and **9AC** (black) in cyclohexane b) Comparison of calculated (red) and measured (black) optical gaps for fluorinated **9AC** compounds

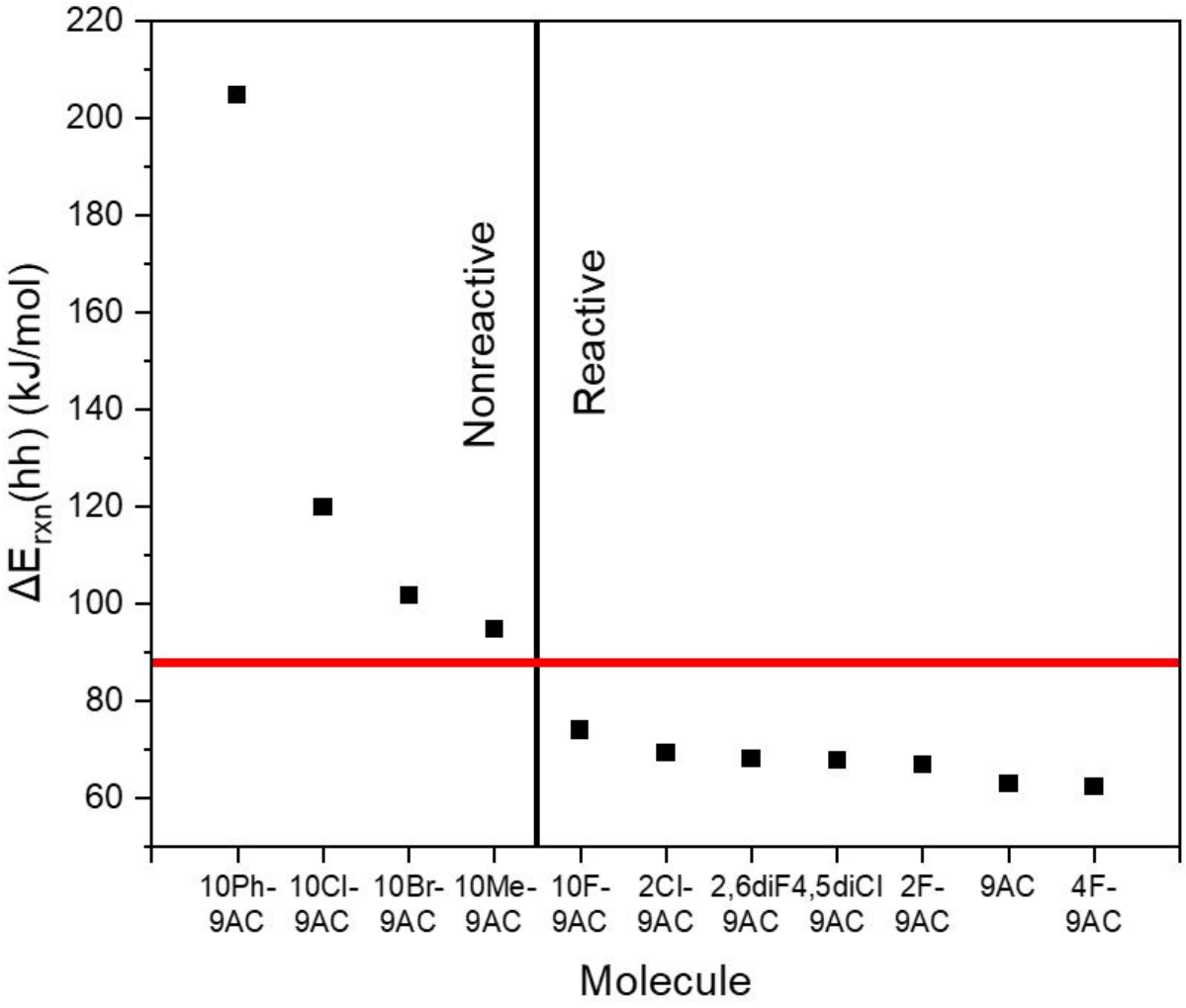

Figure 3. Predicted gas-phase ΔE_{rxn} dimerization energies for various **9AC** derivatives, calculated for monomer pairs. The red line represents the approximate energy threshold above which photodimerization is not observed in the crystal form.

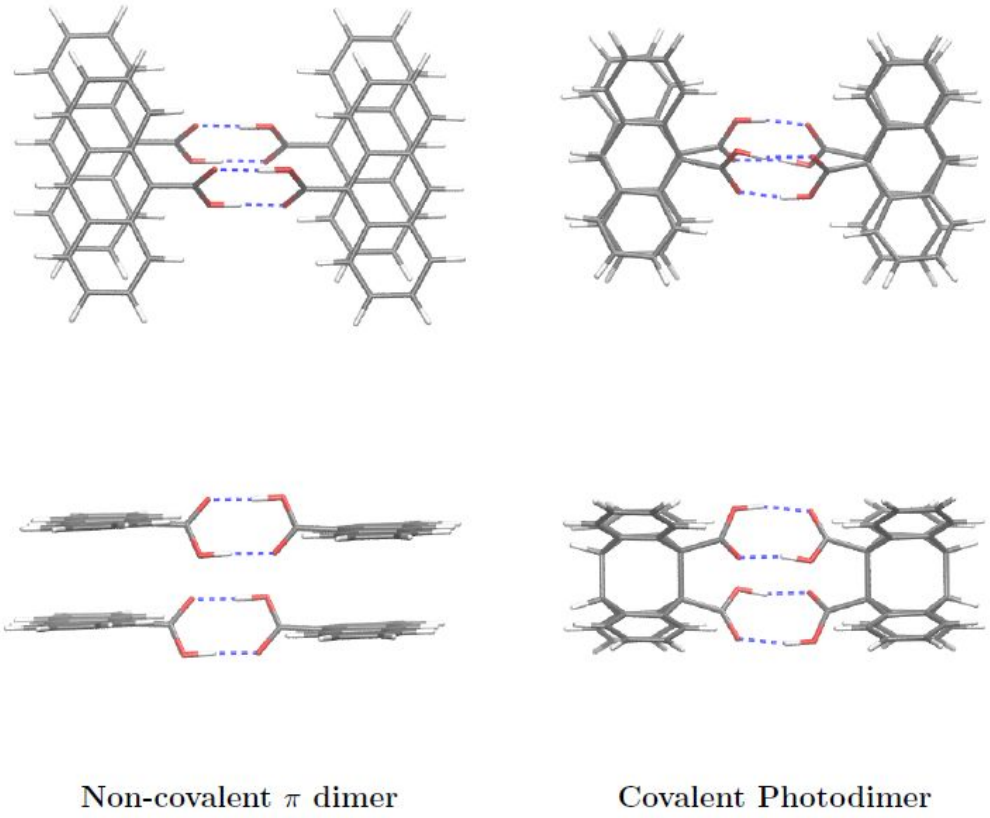

Figure 4. Top and side view of the **9AC** tetramer before and after double photodimerization. The photodimer structure was optimized in the gas phase.

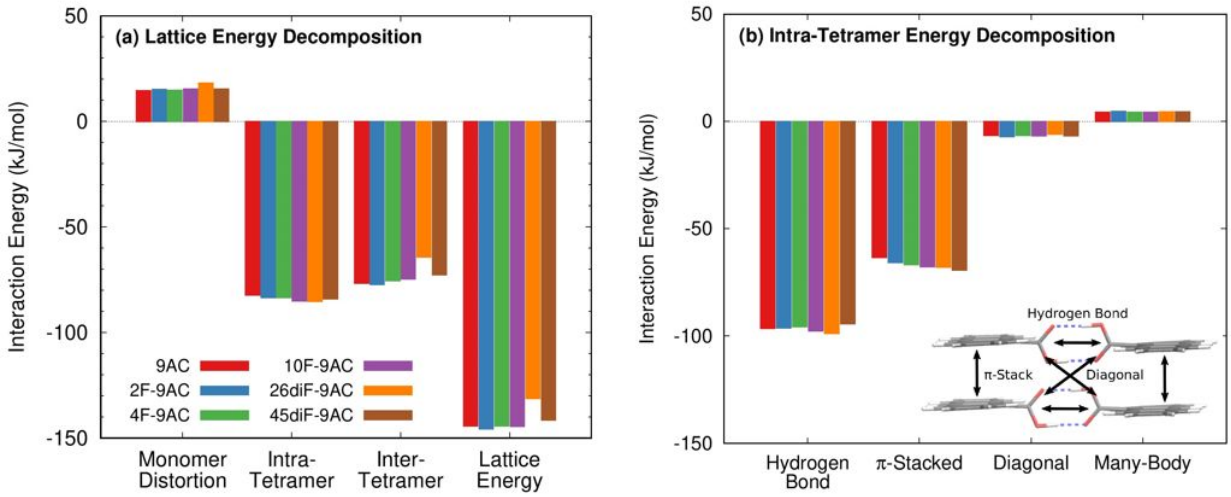

Figure 5. **a)** Effect of fluorine substitution on various lattice energy terms for six different **9AC** derivatives. **b)** Effect of fluorine substation on tetramer energy terms for the same **9AC** derivatives. In all cases, the changes induced by different locations of the F-atom amount to only a few kJ/mol.

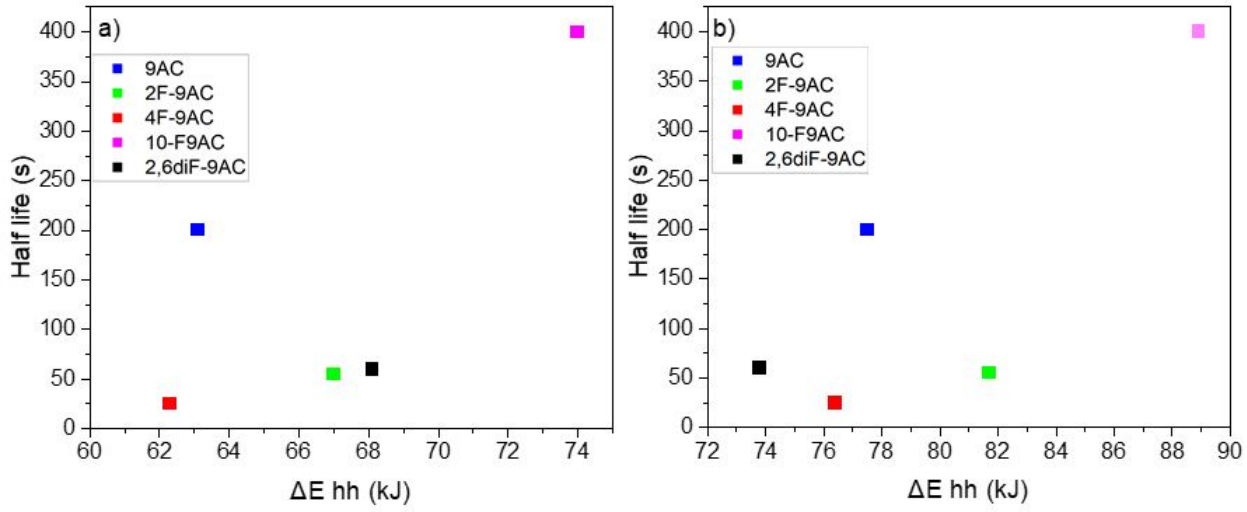

Figure 6. Fluorescence recovery times ($\tau_{1/2}$) taken from reference [23] plotted versus the calculated **a)** dimer and **b)** tetramer photodimerization energies.

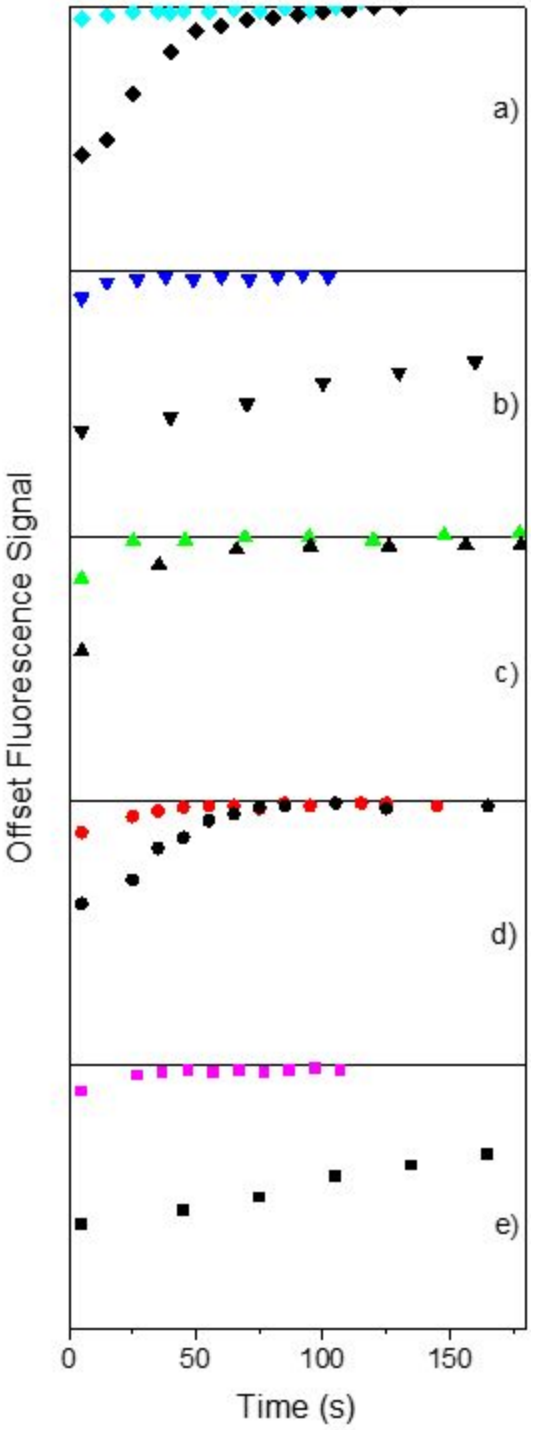

Figure 7. Fluorescence recovery after photobleaching curves for **a) 4F-9AC, b) 10F-9AC, c) 2,6diF-9AC, d) 2F-9AC**, and **e) 9AC** after small (~5% colored symbols) and large (~50% black symbols) photodimer conversions. The data in **a)** is taken from reference [29].

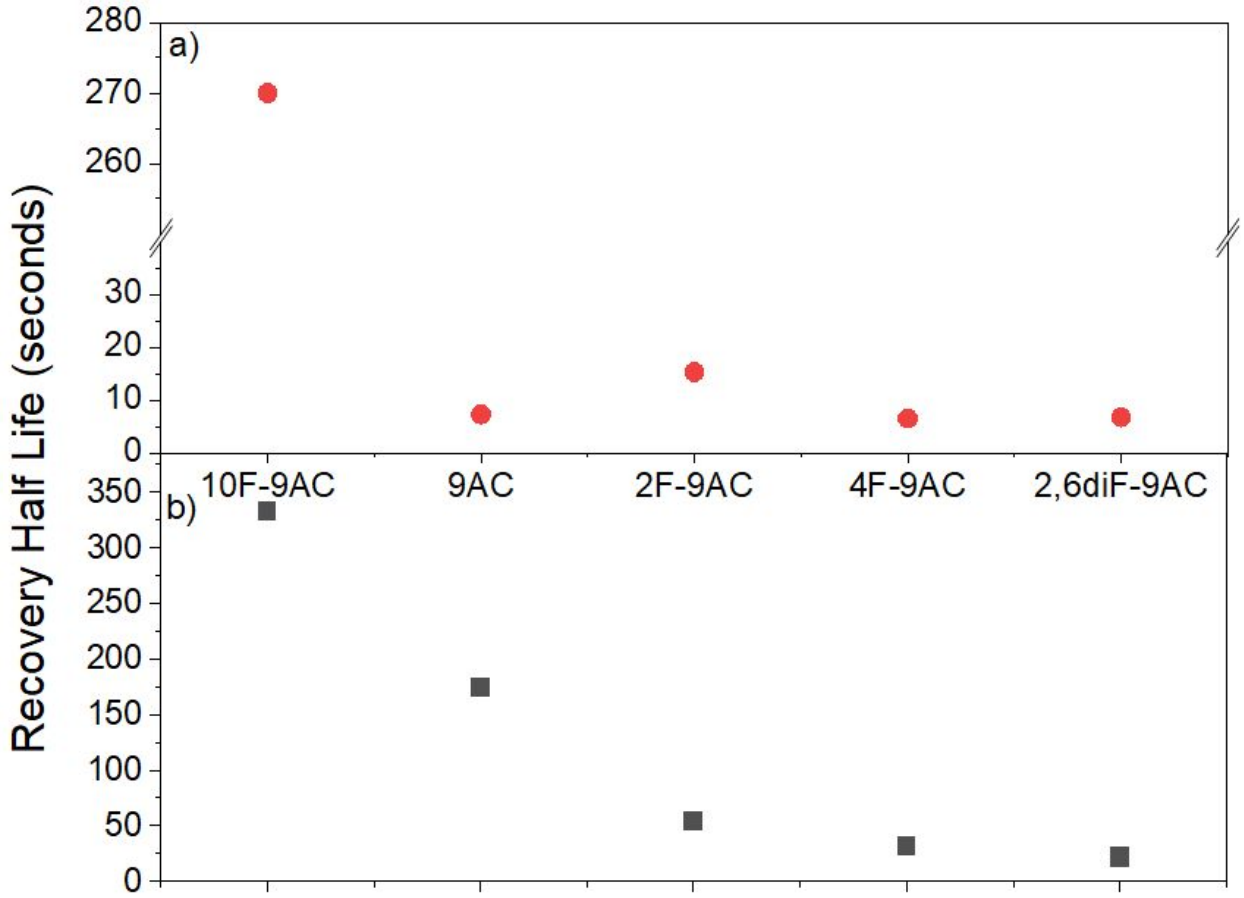

Figure 8. Fluorescence recovery times ($\tau_{1/2}$) for **9AC**, **10F-9AC**, **2F-9AC**, **4F-9AC**, and **2,6diF-9AC** compounds after **a)** small (~5%) photodimer conversion and **b)** large (~50%) photodimer conversion.